Direct measurements and *ab initio* simulations for expanded fluid aluminum in the metal-nonmetal transition range

Jean Clérouin* and Pierre Noiret
CEA-DAM, DIF F-91297 Arpajon, France

Victor N. Korobenko and Anatoly D. Rakhel
Joint Institute of High Temperatures, Russian Academy of Sciences, Izhorskaya 13/19, Moscow 125412, Russia
(Received 3 October 2008; published 15 December 2008)

We have performed direct measurements and quantum molecular-dynamics simulations for expanded aluminum at densities two to nine times lower than the normal solid density and internal energies ranging from 7 to 70 kJ/g. The simulation results were found to be in good agreement with the experimental data and reproduce well the main trends observed in the measured dependencies of the electrical resistivity and pressure versus internal energy along isochores. A systematic study of the optical conductivity spectra, one-particle density of states, and the distributions of the electronic charge over supercell shows that the transition of expanded aluminum to a nonmetallic state takes place close to the density at which the constant volume derivative of the electrical resistivity on internal energy becomes negative.

DOI: 10.1103/PhysRevB.78.224203 PACS number(s): 52.50.Nr, 52.25.Fi, 52.25.Kn, 71.15.Pd

I. INTRODUCTION

When a liquid metal is heated under supercritical pressure so that its density is lowered by a factor of 3–5, one expects that it will continuously pass from the condensed state into a gaseous state. The question is: at which density the expanded metal looses its metallic properties, i.e., changes into a semiconductor, or in the general case, into a nonmetal, and how this transition affects its thermodynamic properties?[1] At present we know about the behavior of mercury and several other metals with sufficiently low critical points, thanks to the classical steady-state techniques.[2,3] For metals with higher critical points, until recently, there were no data obtained by means of direct measurements due to the difficulty of making accurate measurements at high temperatures and pressures.

Recently a experimental technique has been developed that allows direct measurements at temperatures of the order of 10 kK and pressures of the order of 10 kbar. The first results, using this technique, were obtained on aluminum, expanded from the standard solid density by a factor of 6–10 under a pressure $P \gtrsim 20$ kbar.[4] These results have shown that the dependence of the electrical resistivity of aluminum on internal energy along isochores acquires a negative slope at a density four times lower than the standard solid density. It was concluded that such behavior probably indicates transition of aluminum into a nonmetal state. The caloric equation of state (EOS) data measured in that work, i.e., the dependence of pressure on internal energy and density, evidences that this transition is continuous.

However, the data reported in Ref. 4 correspond to a rather narrow range of internal energy and pressure that precludes from a precise determination of the characteristic density at which the constant volume derivative $(\partial\sigma_{dc}/\partial T)_V$ changes its sign (σ_{dc} is the dc conductivity and T is the temperature). Moreover, those data represent results of five successful experiments only that correspond to a relatively high level of the random uncertainty. In this paper we present data obtained in a much larger amount of experiments and for a wider range of pressure and specific internal energy. An effort was made in this work to estimate the systematic uncertainties of the measurements. As a result we can state now that the measurements give the data with an uncertainty (in total the recognized systematic and random) less than 20%.

To interpret the observed behavior of expanded aluminum, we have performed quantum molecular-dynamics (QMD) simulations for the system in a wide range of density and internal energy, including the whole domain where the experimental data were obtained. It is now well accepted that despite some limitations, the QMD simulations have shown their ability in predicting thermodynamic and transport properties of expanded liquid metals and dense metal plasmas.[5–10]

Present QMD simulation results are found to be in fairly good agreement with the experimental data on both the thermodynamic properties and electrical resistivity (up to within the uncertainty of the measurements). Being convinced after this comparison that the QMD simulations provide a reasonable description of expanded aluminum, we have used this microscopic approach to cast light on the physics of the metal-nonmetal (MNM) transition in this substance. In particular, we computed the optical conductivity spectra for different densities and temperatures to reveal the onset of localization for the conducting electrons. Snap shots of the electron-density distributions over the QMD simulation box and the single-particle density of states (DOS) were also analyzed for this purpose.

II. EXPERIMENT

In our experiments an aluminum foil strip of about 16 μm thickness, 6 mm width, and 10 mm length together with a ruby plate of 320 μm thickness is sandwiched between two sapphire plates of 1.6 mm thickness and 10 mm of both width and length (see Fig. 1). The ruby plate is used for the measurements of pressure in the vicinity of the specimen. All parts of the assembly are carefully glued to ensure that

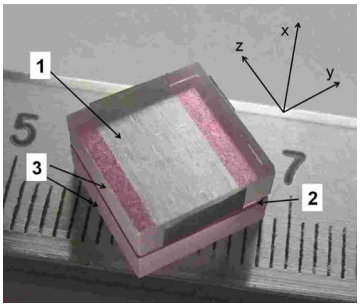

FIG. 1. (Color online) Photograph of an experimental assembly: an aluminum foil strip of 16.0 μm thickness (1) together with a ruby plate (2) of about 320 μm thickness sandwiched (glued by epoxy) between two sapphire plates (3) of 1.6 mm thickness. The bent ends of the foil strip in this experiment are pressed to the electrodes delivering the heating current pulse.

no gaps or cavities exist between the parts (this is very important for an accurate determination of the specimen volume). The specimen is heated by an electrical current pulse so that in less than 1 μs the Joule heat deposited into the specimen achieves four to six times the cohesion energy of aluminum and the density decreases five to nine times. The geometrical dimensions of the experimental assembly and the temporal dependence of the heating current were chosen so that a sufficiently homogeneous heating and a practically one-dimensional (1D) expansion of the foil specimen is realized (the specimen expands mainly in the direction perpendicular to the foil surface, i.e., along the x axis shown in Fig. 1). The proper parameters of the experiments were determined on the basis of 1D magnetohydrodynamic simulations of the pulse Joule heating dynamics.[11]

Diagnostics in these experiments are as follows. The current running through the specimen, the voltage drop across its length, and the pressure near the specimen are measured. From the measured quantities in the case of the uniform and one-dimensional expansion of the specimen, the electrical resistivity, the density, and the internal energy are determined. Hence one obtains the electrical resistivity and pressure both as functions of density and internal energy. A detailed description of the technique can be found in the previous papers.[4,12]

Before passing to the results of the measurements, we estimate some systematic errors not discussed in our previous papers. First of all, we would like to clarify one point in the approach we use to determine the specimen volume. We recall to the reader that we measure the temporal dependence of the pressure near the specimen using the well-known ruby luminescence line shift technique.[13,14] The displacement of the specimen-sapphire interface is calculated by solving the one-dimensional hydrodynamic task regarding movement of piston in a medium in which mechanical properties are known and the pressure applied against the piston is a given function of time. At present, the equation of state of sapphire within the range of elastic compression ($P<125$ kbar) is known with a rather high precision (the uncertainty is less than 1%) that allows us to calculate the specimen volume rather accurately. In the case of an isentropic uniaxial compression the equation of state can be written as a relation

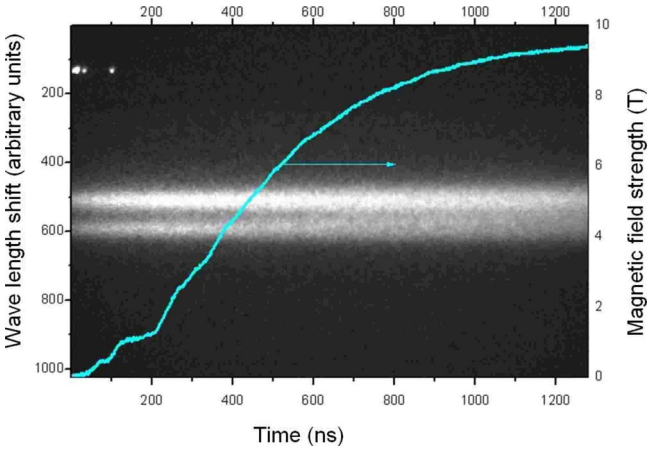

FIG. 2. (Color online) Streak image of a-cut ruby luminescence lines (R_1 and R_2 lines) and a temporal dependence of the magnetic field of the current flowing in a copper strip placed near the ruby plate so that the plate is not subjected to a compression.

between the pressure P and the density ρ in the following form:

$$P = \frac{B}{n}\left[\left(\frac{\rho}{\rho_0}\right)^n - 1\right], \tag{1}$$

where ρ_0 is the normal density of sapphire and the coefficient B and the exponent n are assumed to be constant. The values of these parameters were found by fitting to the data measured in the shock-wave experiments[15] ($\rho_0=3.985$ g/cm^3, $B=499.0$ GPa, $n=3.0$). In fact, the difference in pressure given by Eq. (1) and the analytical equation for the Hugoniot curve obtained from the Rankine-Hugoniot relations and the measured dependence between the particle velocity u and the shock velocity D in sapphire,[15]

$$D = 11.19 + 1.0u, \tag{2}$$

is less than 0.03% that is much smaller than the uncertainty of the measurements in Ref. 15 and Refs. 13 and 14 as well.

Thus, we use the equation of state data obtained in the shock-wave experiments to describe isentropic deformation of sapphire plates in our experiments. We can do that because the entropy change for sapphire upon the shock compression within the range of elasticity is sufficiently small. The term due to the entropy change makes a contribution to the pressure increase that is less than 0.01%.

The next essential point we are going to discuss here is the influence of the magnetic field produced by the heating current on the ruby luminescence line shift and broadening due to Zeeman effect. This effect has become more remarkable in the present experiments because we used electrical current pulses of higher magnitudes to reach a higher level of pressure compared to that in Ref. 4. Several experiments with and without compression of the ruby plate have been performed in the presence of the magnetic field.

In Fig. 2 the effect of the magnetic field on the luminescence line broadening is shown. In this case the ruby plate was not subjected to compression and remained at the atmospheric pressure. The line broadening in the magnetic field

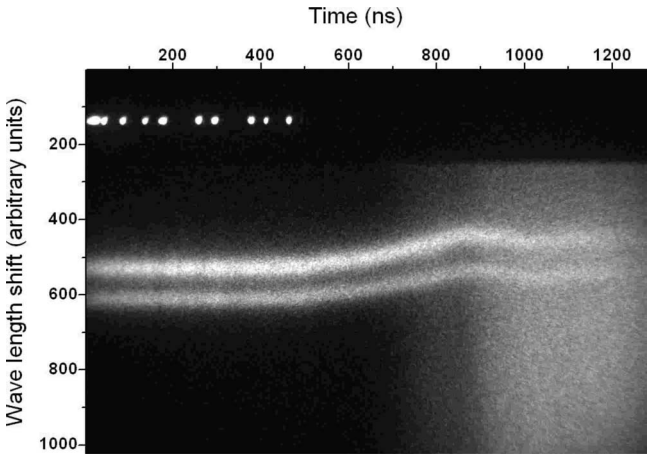

FIG. 3. Streak image of *a*-cut ruby luminescence lines measured in an experiment with compensation of the magnetic field in the middle part of the ruby plate.

higher than about 6 T is evident (the magnetic field of 6 T corresponds in our experiments to a current magnitude of about 60 kA). To reduce the Zeeman effect and therefore to lower the pressure measurement uncertainty, the magnetic field in the middle part of the ruby plate (from where the ruby luminescence is collected) was compensated by a reverse current conductor placed close to the experimental assembly. The geometrical dimensions of the reverse current conductor and the sapphire plates were chosen so that the maximum value of the magnetic field in that place was less than 3 T [according to two-dimensional (2D) simulations]. The luminescence lines measured in an experiment with compensation of the magnetic field in the ruby plate are shown in Fig. 3. In this experiment the ruby plate was a part of the experimental assembly shown in Fig. 1 and therefore was compressed by the expanding aluminum specimen. It is obvious that due to the compensation of the magnetic field in the ruby plate the quality of the luminescence lines remains good.

In Fig. 4 we present distribution of the x component of magnetic field along the y axis. The field is generated by a

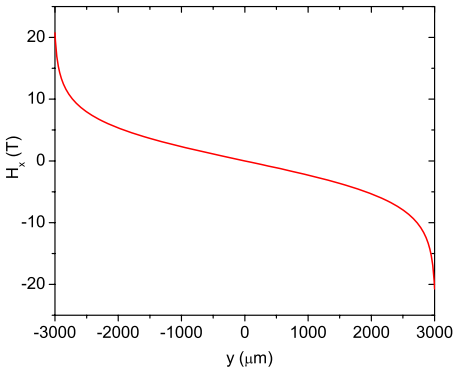

FIG. 4. (Color online) Distribution of the x component of the magnetic field caused by a homogeneous current of 100 kA magnitude flowing through the specimen along the z axis. The distribution is presented for the surface $x=0$ that is a symmetry plane for the specimen.

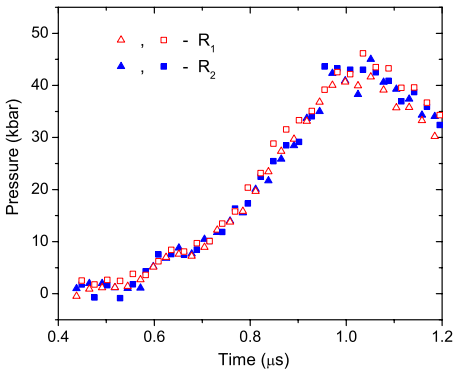

FIG. 5. (Color online) Pressure vs time for two experiments with different concentrations of chromium. Triangles show the data obtained for the two R lines in an experiment with the concentration of chromium of 0.28% and the squares correspond to a concentration of 0.15%

homogeneous current of 100 kA magnitude flowing through the specimen along the z axis (see Fig. 1 for the coordinate system used). As one can see, the magnitude of the field reaches about 21 T near the specimen sides; for an infinitely wide specimen the H_x component is absent. One may expect that this field causes an electromotive force resulting in an inhomogeneous contribution to the z component of the electric field and therefore inhomogeneous heating. Estimates show that this effect produces an inhomogeneity in the heat dissipated at the specimen sides that is less than 5%.

We have investigated also the effect of doping of sapphire with chromium ions on the ruby pressure scale. In Fig. 5 the temporal dependencies of pressure for two experiments with different concentration of chromium are shown. These experiments correspond to concentrations of Cr_2O_3 (by weight) of 0.28% and 0.15%. As one can see, deviation of the data points from an average value for a certain experiment and line is comparable with the difference between the pressure values for the R_1 and R_2 lines (± 2 kbar). Thus, we could not see the influence of the chromium concentration on the pressure measurement results. Consequently we can conclude that the uncertainty caused by the difference of the chromium concentration in our experiments and in the experiments in Refs. 13 and 14 (where the ruby pressure scale has been established for uniaxial compression of sapphire and where the concentrations were 0.4% and 0.5%, correspondingly) is less than about 6%.

In conclusion we present estimates for the temperature increase in the ruby plate due to the heat transfer from the hot specimen. The point is that the ruby luminescence line shift is very sensitive to temperature.[14] Our estimates are based on the following assumptions. The thermal diffusivity of sapphire χ strongly decreases with temperature and, for liquid sapphire, becomes of the order of 0.01 cm^2/s.[16] Hence, for a typical time of the measurements $\tau \sim 1$ μs, the thickness of a molten layer of ruby is of the order of $\sqrt{\chi\tau} \sim 1$ μm. This distance is very small compared with the ruby plate thickness and therefore we can neglect this displacement. Thus, the task can be posed as follows. At the hot boundary of the ruby plate, a fixed value of temperature is held that is equal to the melting temperature of sapphire. At

zero time $T(x,0)=300$ K at all points except the boundary. What is the temperature distribution at the subsequent times? The calculations show that during 1 μs a temperature increase of more than 10 K takes place in a layer of about 12 μm thickness. Such heating practically does not affect our pressure measurement results because the thickness of the ruby plates used in our experiments is much larger.

III. QMD SIMULATIONS

The simulations were performed using projector augmented wave pseudopotentials[17] with the electronic structure package VASP developed at the University of Vienna.[18] We used pseudopotentials with three active electrons ($3s^2 3p^1$) and with a cutoff energy of 318 eV. Inclusion of more electrons is needed at much higher pressures[19] when the core electrons ($2p^6$) are subjected to ionization.

The exchange-correlation potential in the Kohn-Sham equations was treated at the level of the local-density approximation[20] (LDA) using the Ceperley-Alder parametrization.[21] During the molecular-dynamics simulations, the Brillouin zone was sampled at the Γ point. We used more refined k-point sampling such as 2^3 and 3^3 in the Monkhorst-Pack scheme[22] for the optical conductivity calculations. The ionic trajectories were generated for 62 atoms of aluminum in the supercell during 2 ps (1000 time steps of 2 fs each) after equilibration. Molecular-dynamics simulations were performed in the isokinetic ensemble to make temperature control easier. To decrease the equilibration time, the initial conditions for each temperature were taken from the previous simulation run performed at lower temperature. We assumed that equilibrium was reached when the pressure versus time demonstrated a steady average value with a sufficient number of oscillations around it (five to ten oscillations). We also tested the convergence of the simulations by varying the number of atoms in the simulation box. In particular, runs with 32 ions in the box were performed but without noticeable change in the results. Uncertainties in the pressure (the error bars) were obtained by calculating the statistical fluctuations along the QMD simulations.

From the knowledge of the Kohn-Sham orbitals ψ_n, energies ϵ_n, and occupation numbers f_n, the conductivity was computed on selected ionic configurations using the Kubo-Greenwood formulation,[23,24]

$$\sigma(\omega) = \frac{2\pi}{3\omega}\frac{1}{\Omega}\sum_{n,m,\alpha}\sum_{\boldsymbol{k}} W(\boldsymbol{k})(f_n - f_m)|\langle\psi_n^{\boldsymbol{k}}|\nabla_\alpha|\psi_m^{\boldsymbol{k}}\rangle|^2 \times \delta(\epsilon_m^{\boldsymbol{k}} - \epsilon_n^{\boldsymbol{k}} - \hbar\omega), \quad (3)$$

where $\boldsymbol{k}$ and $W(\boldsymbol{k})$ are the wave vectors and their weights in the Brillouin zone, ∇_α is the velocity operator in each direction ($\alpha=x,y,z$) between two states n and m with occupation numbers f_n and f_m, and Ω is the supercell volume. The dc conductivity is obtained by taking the zero-frequency limit of $\sigma(\omega)$. We also checked that the frequency sum rule,

TABLE I. QMD simulation results. The results were obtained for 2^3 k-point sampling of the Brillouin zone.

Volume V/V_0	Energy (kJ/g)	Pressure (kbar)	T (kK)	σ_{dc}^{-1} ($\mu\Omega$ m)
1.93	7.52	2.35	5	1.09
1.93	9.6	32.4	7	1.16
1.93	12.0	59.7	10	1.23
1.93	17.4	112.3	15	1.33
1.93	23.5	167.7	20	1.43
1.93	30.5	232.8	25	1.43
1.93	37.6	289.4	30	1.45
1.93	53.4	427.1	40	1.54
2.7	10.88	14.02	7.5	2.38
2.7	13.3	29.2	10	2.58
2.7	14.95	43.41	11.6	2.7
2.7	18.8	62.4	15	2.76
2.7	25.3	100.2	20	2.86
2.7	32.6	139.3	25	2.88
2.7	40.3	179.8	30	2.80
2.7	55.8	268.1	40	3.33
4.0	14.7	15.6	10	6.94
4.0	20.5	34.3	15	7.19
4.0	27.1	57.6	20	6.67
4.0	34.3	80.4	25	6.25
4.0	42.7	109.7	30	
4.0	60.0	164.4	40	5.45
5.4	15.4	12.0	10	15.4
5.4	21.4	25.77	15	16.7
5.4	28.5	40.8	20	15.3
5.4	36.6	58.2	25	10.6
5.4	44.7	74.8	30	9.43
5.4	62.5	114.0	40	7.81

$$S = \frac{2m\Omega}{\pi e^2 N_e}\int_0^\infty \sigma(\omega)d\omega = 1, \quad (4)$$

was satisfied with a given accuracy (95%) by adding enough electronic bands in the computation, where e and m are the electron charge and mass, respectively, and N_e is the number of the active electrons in the supercell.

To compute the reference state energy, we simulated aluminum in the solid state at $T=300$ K and $\rho=2.7$ g/cm^3 in the fcc phase with 108 atoms in the supercell. As a result we got an internal energy value of -4.10 eV/atom, which must be subtracted from the energy values obtained in the QMD simulations to compare these results with the measurement data. The results of the QMD simulations are given in Tables I–III.

IV. RESULTS

The equation of state data for expanded aluminum in the MNM transition range (pressure versus internal energy along

TABLE II. Experimental data points.

Volume V/V_0	Energy (kJ/g)	Pressure (kbar)	σ_{dc}^{-1} ($\mu\Omega$ m)
1.93	8.51	12.6	1.66
1.93	8.83	11.6	1.70
1.93	8.49	24.2	1.49
1.93	9.11	25.5	1.54
1.93	9.29	23.5	1.51
1.93	8.95	30.9	1.35
1.93	9.51	34.1	1.47
1.93	9.36	32.7	1.47
1.93	8.96	25.4	1.55
1.93	9.67	34.4	1.41
1.93	9.89	38.0	1.37
1.93	8.20	20.6	1.41
1.93	7.19	18.2	1.29
1.93	8.47	19.2	1.46
1.93	10.25	38.2	1.50
1.93	9.16	37.3	1.38
2.7	16.7	36.5	4.24
2.7	13.7	21.8	4.20
2.7	13.8	18.1	3.64
2.7	15.7	34.7	3.33
2.7	17.3	39.2	3.92
2.7	16.8	34.1	3.68
2.7	17.4	48.2	3.44
2.7	18.3	54.2	3.55
2.7	17.1	48.6	3.49
2.7	15.1	33.6	3.49
2.7	15.3	34.4	3.24
2.7	19.1	51.3	3.39
2.7	19.7	51.6	3.37
2.7	13.2	28.9	3.25
2.7	13.1	26.7	3.24
2.7	14.3	27.6	3.40
2.7	18.3	54.4	3.33
2.7	17.7	52.6	3.36

TABLE III. Experimental data points.

Volume V/V_0	Energy (kJ/g)	Pressure (kbar)	σ_{dc}^{-1} ($\mu\Omega$ m)
4.0	20.6	28.2	9.80
4.0	20.5	27.3	8.59
4.0	27.3	49.4	7.70
4.0	29.3	48.9	8.39
4.0	28.0	42.7	8.92
4.0	27.6	43.0	8.20
4.0	32.3	58.4	7.76
4.0	34.2	70.5	7.53
4.0	25.1	44.4	8.24
4.0	24.6	42.6	7.56
4.0	35.1	64.0	6.83
4.0	22.5	38.4	8.43
4.0	22.3	37.3	8.14
4.0	24.0	34.0	8.38
4.0	33.4	66.2	7.32
4.0	32.8	65.5	7.39
5.4	26.5	26.1	15.50
5.3	26.0	29.5	13.80
5.4	38.7	49.6	11.57
5.4	41.4	47.4	12.27
5.4	37.9	42.7	12.26
5.4	46.0	61.0	10.99
5.4	49.5	71.6	9.25
5.4	35.0	45.2	12.65
5.4	50.0	62.4	9.76
5.4	30.2	41.2	13.49
5.4	30.6	37.0	12.83
5.4	32.5	39.4	13.15
5.4	46.8	66.7	10.44
5.4	46.7	67.3	10.73
9.0	58.4	47.1	17.5
9.0	57.1	46.6	18.1
9.0	48.9	36.5	19.0
9.0	72.1	54.9	13.3
9.0	40.7	38.2	21.6
9.0	43.9	36.0	20.7
9.0	66.5	67.0	14.7
9.0	67.3	67.4	15.1

five isochores) are shown in Fig. 6. The isochores correspond to the following relative volume values: $V/V_0=1.93$, 2.7, 4, 5.4, and 9 ($V_0=10$ cm^3/mol). As one can see, the experimental data obtained in this work are in a reasonable agreement with those in Ref. 4. General agreement is also observed between the data and the present QMD simulation results. Some discrepancy seems to appear at the relative volume values $V/V_0=4$ and 5.4 but the difference does not exceed 20%, which is an estimated uncertainty of the pressure measurements.

The electrical resistivity versus internal energy along the isochores is shown in Fig. 7. As in the case of the pressure dependence, we have a good agreement between the simulation and experimental results. The present experimental data also agree well with the measurement results in Ref. 4. As one can see, the QMD data for the electrical resistivity reproduce the general trend observed in the experiments. At the low relative volume values, the resistivity increases with the internal energy along isochores and hence with temperature, demonstrating a typical behavior of a metal having an odd number of conducting electrons per atom. At larger expansions the dependence is opposite; the resistivity decreases with internal energy, which resembles the behavior of a semiconductor. Our calculated resistivity values for $V/V_0=1.93$ are close to those obtained recently by Faussurier *et*

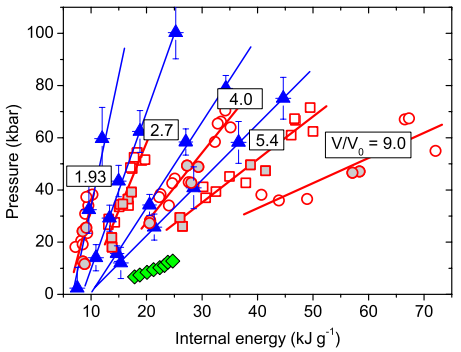

FIG. 6. (Color online) Pressure versus internal energy along five isochores (V/V_0=1.93, 2.7, 4.0, 5.4, 9.0). The open red circles and squares represent these work's experimental data, the filled red circles and squares are those in Ref. 4, the blue triangles give the QMD simulation results, and the green diamonds are the experimental results in Ref. 25 for V/V_0=9. The red and blue lines are linear fits of our experimental data and the simulation results along isochores correspondingly.

al.[26] by means of a hard-sphere variational theory combined with a Kubo-Greenwood evaluation of conductivity. A satisfactory agreement is also seen between the present experimental results (when extrapolated to the lower internal energy values) and those in Ref. 25 for both the EOS and the electrical resistivity data. It should be noted, nevertheless, that the slope in the dependence of the resistivity on internal energy obtained in that work differs strongly from the value measured in present experiments. The point is that the experimental results in Ref. 25 are obtained by a technique whose precision is not still well estimated. Therefore the slope in the dependence of the resistivity vs internal energy for these data is not in fact a rather reliable quantity.

QMD results for V/V_0=9 in Ref. 25 are not shown here because the present experimental results, as well as recent QMD simulations,[27] evidence that the resistivity values in Ref. 25 are underestimated by about 50%. Test simulations at this volume with 64 particles and a much larger amount of orbitals (up to 2000) also confirm this conclusion. A more accurate computation of the resistivity values for this volume, for example, with 20% uncertainty, requires much more computer time, which exceeds our possibilities.

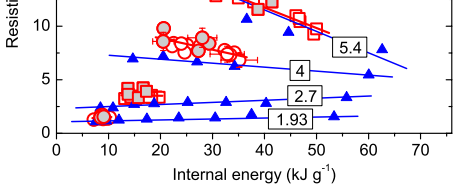

FIG. 7. (Color online) Electrical resistivity versus internal energy along five isochores. The meaning of the symbols is the same as in Fig. 6.

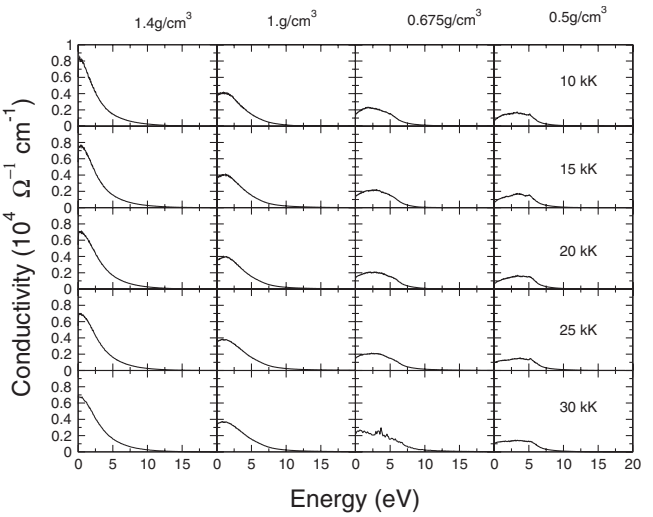

FIG. 8. Optical conductivity spectra for four selected values of density and five values of temperature.

V. OPTICAL CONDUCTIVITY SPECTRA AND THEIR INTERPRETATION

The QMD results on the optical conductivity are shown in Fig. 8 for five selected values of the temperature and four density values. For a given temperature, we observe a continuous transformation of the optical conductivity spectrum when the density is lowered. Its shape changes from a typical form of a good Drude metal to that of a semiconductor at the lowest density. The maximum in the optical conductivity spectrum, which is located at zero frequency at normal density, shifts to positive-energy values with increasing of the relative volume. Hence, the system acquires a nonzero characteristic frequency $\omega_{\max}$, corresponding to the value at the maximum. Such behavior indicates the onset of localization for the conducting electrons. A remarkable shift of the maximum, i.e., when $\hbar\omega_{\max} > kT$ (k is the Boltzmann constant), takes place for expansion V/V_0=4.0 at which the dc conductivity, according to the experimental results, already increases with temperature (see Fig. 7). This general evolution of the optical conductivity shape is very similar to that discussed in Ref. 28 and has been observed in earlier experiments for expanded mercury.[3,29]

At a constant density ρ=1.4 g/cm^3 (V/V_0=1.93), we observe a metal-like behavior at all temperatures considered, characterized by a monotonic decrease in the dc conductivity with temperature. At the lowest density ρ=0.5 g/cm^3 (V/V_0=5.4), the dc conductivity, being much smaller in the magnitude than the metallic values, increases with temperature.

Aluminum is a simple metal and at normal density its electrical properties are well described by the Drude model. Therefore we can use this model for interpretation of the optical conductivity spectra in the metallic state, i.e., at ρ =1.4 g/cm^3. The optical conductivity within this model is given by the formula

$$\sigma_D(\omega) = \frac{ze^2\tau/m}{1+\omega^2\tau^2}, \tag{5}$$

where z is the conducting electron number density and τ is a relaxation time. In the low energy range $\hbar\omega \lesssim 5$ eV, we ad-

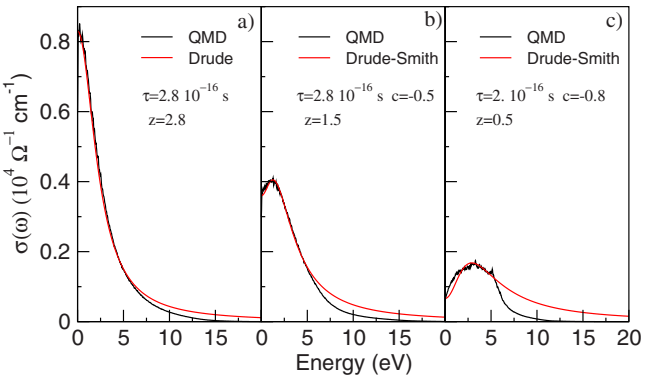

FIG. 9. (Color online) Optical conductivity spectra for three relative volume values: (a) $V/V_0=1.93$ and $T=10$ kK, (b) $V/V_0=2.7$ and $T=15$ kK, and (c) $V/V_0=5.4$ and $T=10$ kK.

justed the relaxation time τ and the number density of the conducting electrons z to get the best fit of the optical conductivity spectrum obtained from the QMD simulations. An example of the fit is shown in Fig. 9(a) for $T=10$ kK. In this case we got a relaxation time $\tau=2.8\times10^{-16}$ s and the number of the conducting electrons per ion $z=2.8$. Thus, at this density, $\rho=1.4$ g/cm^3, aluminum is still a good metal with almost the same number of conducting electrons as in normal conditions.

When the density is lowered, the central peak of the optical conductivity spectrum is shifted and the Drude formula cannot be applied to fit the QMD results. For these densities the Drude-Smith model[30] is more appropriate. This model is a formal generalization of the classical Drude model with the aim of including the memory effects of the successive collisions. Instead of having a monotonic decay for the current autocorrelation function, this formula allows also for a negative anticorrelation, which reflects the average velocity reversal after successive collisions. This model was successfully used to describe the frequency dependence of the real and imaginary parts of the optical conductivity for expanded liquid mercury.[30] The one collision time formulation for this model reads

$$\sigma_{DS}(\omega)=\frac{n^*e^2\tau/m}{1+\omega^2\tau^2}\left[1+\frac{c(1-\omega^2\tau^2)}{(1+\omega^2\tau^2)}\right], \qquad (6)$$

where c is a parameter of the memory effect. It is zero for the classical Drude model and becomes negative (between 0 and −1) when the central peak is shifted to positive-energy values. The value $c=-1$ corresponds to vanishing dc conductivity associated with a wide resonance in the energy range of 1–2 eV. In Fig. 9(b) we present an optical conductivity spectrum obtained by means of this formula when the corresponding parameters are chosen to fit the QMD results for $T=15$ kK and $V/V_0=2.7$. The central peak is now shifted to about 1.5 eV, and a good fit is obtained for $c=-0.5$, $\tau=2.8\times10^{-16}$ s, and $z=1.5$. This shift and the depression of the dc conductivity become more and more pronounced when the density is lowered, as shown in Fig. 9(c) for $T=10$ kK and $V/V_0=5.4$. In this last case, we see that, while the low-frequency part of the optical conductivity is reproduced satisfactorily, the high energy part is remarkably overestimated. It is interesting to note that at $V/V_0=2.7$ a great part of conducting electrons becomes localized (about 50%) and at the larger expansion, $V/V_0=5.4$, the number of conducting electrons per ion (in the Drude description) is reduced to 0.5.

VI. DISCUSSION

The MNM transition phenomenon in expanded fluid metals is a fundamental and long-standing issue that is especially difficult for theoretical treatment due to the concurrence of the density and temperature effects. Based on the experimental observations of different metallic systems in the MNM transition range, an empirical value of the minimum dc conductivity of a standard metal was determined. A well accepted value ranges between 3000 and 5000 $(\Omega\ \mathrm{cm})^{-1}$ (see Ref. 31). For expanded aluminum we are able to determine this value based on its optical conductivity spectra (Fig. 8). In Sec. V we came to the conclusion that the states along isochore $V/V_0=1.93$ correspond to a good Drude metal while at larger expansions the maximum in the optical conductivity spectra shifts to the positive-energy values and a remarkable part of the conducting electrons becomes localized, and therefore the corresponding states are nonmetallic. Thus, the minimum metallic conductivity for aluminum is higher than 4000 $(\Omega\ \mathrm{cm})^{-1}$ but it is lower than the dc conductivity at $V/V_0=4$, i.e., 8000 $(\Omega\ \mathrm{cm})^{-1}$. It should be noted also that even for the isochore $V/V_0=2.7$ the simulation results still demonstrate a negative value of $(\partial\sigma_{\mathrm{dc}}/\partial T)_V$. Hence, we can conclude that indication of negative value of the derivative alone is not enough to relate a state to a metal. For a larger expansion $V/V_0=4$, the corresponding states are obviously nonmetallic because the measured conductivity values, 1300–1000 $(\Omega\ \mathrm{cm})^{-1}$, are noticeably lower than the minimum metallic conductivity value and the derivative $(\partial\sigma_{\mathrm{dc}}/\partial T)_V$ becomes positive and sufficiently large in the absolute value to be measured in our experiments.

Another way to characterize the MNM transition in expanded aluminum is the opening of a gap in the electron DOS. In Fig. 10 we present the DOS calculated for a given instantaneous ionic configuration with a broadening of 0.05 eV. At a density of 0.5 g/cm^3 we observe a depression in the DOS in the vicinity of the Fermi level (which, in fact, develops already at density $V/V_0=4.0$). But this depression becomes smeared out as the temperature increases and does not correspond to a real gap. We must go to a much lower density (0.1 g/cm^3) to observe the formation of a real gap of about 2 eV magnitude.

To describe the microscopic behavior of the system, it is not enough to think in terms of a homogeneous system. Expanded fluid aluminum in the metal-nonmetal transition range represents a strongly inhomogeneous system. To demonstrate this, we present in Fig. 11 the isosurfaces of the electronic density over the supercell for two levels: $n_e=0.094$ Å^{-3} that is close to the average electron density at expansion $V/V_0=1.93$ [top pictures, (a) and (b)] and $n_e=0.034$ Å [bottom pictures, (c) and (d)]. The isosurfaces are presented for two relative volumes: $V/V_0=1.93$ [left pictures, (a) and (c)] and $V/V_0=5.4$ [right pictures, (b) and (d)].

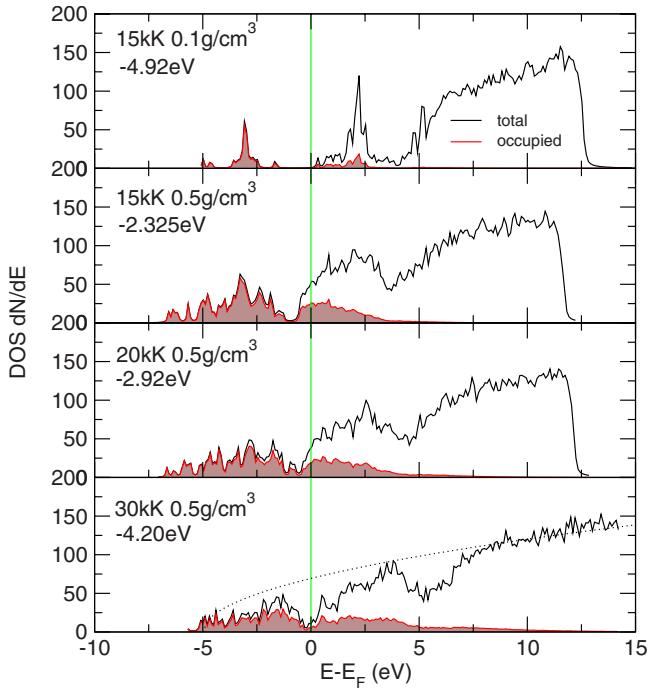

FIG. 10. (Color online) Single particle density of states for two densities of expanded aluminum and three values of temperature. The values of density, temperature, and the Fermi level E_F (in eV) are indicated in the legends. The dotted line is the free-electron-gas density of states.

For the highest electronic density [top figures, (a) and (b)], we observe a transition from a connected network [upper left, (a)] to a disconnected one [upper right, (b)]. This transition corresponds to the classical view of the localization process when the metallic conductivity is due to the formation of percolating paths. More interesting is the representation for the lower-level electronic density which corresponds almost to the third of the average density at $V/V_0=1.93$ [bottom figures, (c) and (d)]. At the expansion $V/V_0=5.4$ [lower right, (d)], there is not much difference compared with the upper right figure. On the contrary at $V/V_0=1.93$ [lower left, (c)], we observe that the electronic density becomes distributed between the nuclei forming a conducting manifold. For this level of electronic density, the expansion of the system causes a topological change in the surface of constant electronic density.

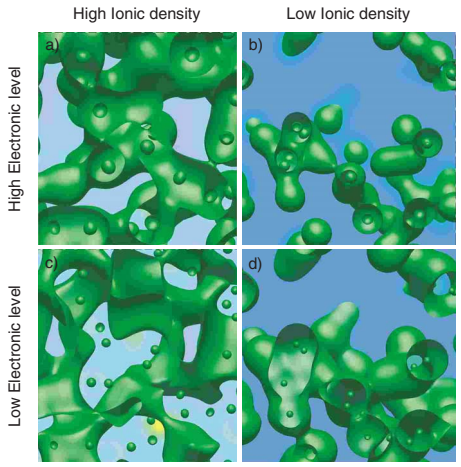

FIG. 11. (Color online) Snap shots of the constant electronic number density surfaces for expansions $V/V_0=1.93$ (left pictures, a and c) and $V/V_0=5.4$ (right pictures, b and d) for two levels of the electronic density: $n_e=0.094$ Å^{-3} (top pictures, a and b) and $n_e=0.034$ Å^{-3} (bottom pictures, c and d). Temperature for all cases is $T=10$ kK. The small spheres represent the electron density in the internal regions (cores).

VII. CONCLUSION

We have performed direct measurements and QMD simulations for expanded fluid aluminum in a wide range of densities and internal energies. The simulation results for the dependencies of pressure and resistivity on internal energy along isochores are in a good agreement with the experimental data. The properties of the system were analyzed through the computation of the optical conductivity spectra, the single-particle density of states, and the distribution of the electronic density over the supercell. This analysis confirms that, in the range of the relative volumes where the dc conductivity of expanded aluminum along isochores acquires a positive slope, the system looses its metallic properties.

ACKNOWLEDGMENTS

The experimental part of this work was performed under the financial support of the Commissariat a L'Energie Atomique (CEA/DAM) uncer Contract No. 0606M and the Presidium of Russian Academy of Sciences in the framework of the program "Thermophysics and mechanics of high-powered energetic actions." We want also to thank C. Starret for reading the paper and some corrections made in the language.

*jean.clerouin@cea.fr

[1] Y. B. Zel'dovich and L. D. Landau, Zh. Eksp. Teor. Fiz. **14**, 32 (1944), in Russian.
[2] I. K. Kikoin and A. P. Senchenkov, Fiz. Met. Metalloved. **24**, 843 (1967), in Russian.
[3] F. Hensel, Philos. Trans. R. Soc. London, Ser. A **356**, 97 (1998).
[4] V. N. Korobenko and A. D. Rakhel, Phys. Rev. B **75**, 064208 (2007).
[5] G. Kresse and J. Hafner, Phys. Rev. B **55**, 7539 (1997).
[6] M. P. Desjarlais, J. D. Kress, and L. A. Collins, Phys. Rev. E **66**, 025401(R) (2002).
[7] V. Recoules, P. Renaudin, J. Clérouin, P. Noiret, and G. Zérah, Phys. Rev. E **66**, 056412 (2002).
[8] J. Clérouin, P. Renaudin, Y. Laudernet, P. Noiret, and M. P. Desjarlais, Phys. Rev. B **71**, 064203 (2005).
[9] P. Renaudin, V. Recoules, P. Noiret, and J. Clérouin, Phys. Rev. E **73**, 056403 (2006).
[10] J. Clérouin, P. Renaudin, and P. Noiret, Phys. Rev. E **77**, 026409

(2008).
[11] V. N. Korobenko, A. D. Rakhel, A. I. Savvatimski, and V. E. Fortov, Plasma Phys. Rep. **28**, 1008 (2002).
[12] V. N. Korobenko, A. D. Rakhel, A. I. Savvatimski, and V. E. Fortov, Phys. Rev. B **71**, 014208 (2005).
[13] P. D. Horn and Y. M. Gupta, Phys. Rev. B **39**, 973 (1989).
[14] X. A. Shen and Y. M. Gupta, Phys. Rev. B **48**, 2929 (1993).
[15] L. M. Barker and R. E. Hollenbach, J. Appl. Phys. **41**, 4208 (1970).
[16] V. D. Golyshev and M. A. Gonik, Akademiia Nauk USSR Izvestiia, Seria Fizicheskaia **52**, 1896 (1988), in Russian.
[17] G. Kresse and D. Joubert, Phys. Rev. B **59**, 1758 (1999).
[18] G. Kresse and J. Hafner, Phys. Rev. B **47**, R558 (1993).
[19] S. Mazevet, F. Lambert, F. Bottin, G. Zérah, and J. Clérouin, Phys. Rev. E **75**, 056404 (2007).
[20] The choice between LDA and generalized gradient approximation (GGA) was decided by computing equilibrium properties of solid aluminum in fcc phase. Moreover, we believe that at high temperature the effect of the exchange-correlation approximation becomes less crucial.
[21] D. M. Ceperley and B. J. Alder, Phys. Rev. Lett. **45**, 566 (1980).
[22] H. J. Monkhorst and J. D. Pack, Phys. Rev. B **13**, 5188 (1976).
[23] R. Kubo, J. Phys. Soc. Jpn. **12**, 570 (1957).
[24] D. A. Greenwood, Proc. Phys. Soc. Jpn. **71**, 585 (1958).
[25] V. Recoules, J. Clérouin, P. Renaudin, P. Noiret, and G. Zérah, J. Phys. A **36**, 6033 (2003).
[26] G. Faussurier, C. Blancard, and P. L. Silvestrelli, Phys. Rev. B **77**, 155126 (2008).
[27] S. Mazevet, M. P. Desjarlais, L. A. Collins, J. D. Kress, and N. H. Magee, Phys. Rev. E **71**, 016409 (2005).
[28] G. Faussurier, C. Blancard, P. Renaudin, and P. L. Silvestrelli, Phys. Rev. B **73**, 075106 (2006).
[29] H. Ikezi, K. Schwarzenegger, A. L. Simons, A. L. Passner, and S. L. McCall, Phys. Rev. B **18**, 2494 (1978).
[30] N. V. Smith, Phys. Rev. B **64**, 155106 (2001).
[31] V. F. Gantmakher, *Electrons in Disordered Media* (Fizmatlit, Moscow, 2003), p. 174, in Russian.